



# A quantum-corrected Monte Carlo study on quasi-ballistic transport in nanoscale MOSFETs

Tsuchiya, Hideaki

Fujii, Kazuya

Mori, Takashi

Miyoshi, Tanroku

---

## (Citation)

IEEE Transactions on Electron Devices, 53(12):2965-2971

## (Issue Date)

2006-12

## (Resource Type)

journal article

## (Version)

Version of Record

## (URL)

<https://hdl.handle.net/20.500.14094/90000439>



# A Quantum-Corrected Monte Carlo Study on Quasi-Ballistic Transport in Nanoscale MOSFETs

Hideaki Tsuchiya, *Senior Member, IEEE*, Kazuya Fujii, Takashi Mori, and Tanroku Miyoshi, *Member, IEEE*

**Abstract**—In this paper, the authors study a quasi-ballistic transport in nanoscale Si-MOSFETs based upon a quantum-corrected Monte Carlo device simulation to explore an ultimate device performance. It was found that, when a channel length becomes shorter than 30 nm, an average electron velocity at the source-end of the channel increases due to ballistic transport effects, and then, it approaches a ballistic limit in a sub-10-nm regime. Furthermore, the authors elucidated a physical mechanism creating an asymmetric momentum distribution function at the source-end of the channel and the influences of backscattering from the channel region. The authors also demonstrated that an electron injection velocity at a perfectly ballistic transport is independent of the channel length and corresponds well to a prediction from Natori's analytical model.

**Index Terms**—Nanoscale MOSFET, quantum effects, quantum-corrected Monte Carlo (MC) simulation, quasi-ballistic transport.

## I. INTRODUCTION

TO ACHIEVE a continuous improvement in drive current of Si-MOSFETs as the International Technology Roadmap for Semiconductors requires [1], carrier-velocity enhancement utilizing ballistic transport, combined with the use of high-mobility channel materials, is considered to be necessary. With the significant advances in lithography technology, a channel length of Si-MOSFET continues to shrink rapidly down to a sub-10-nm regime [2], and the nanoscale channel lengths open up a possibility to realize a quasi-ballistic operation of MOSFETs. The device physics of the quasi-ballistic MOSFETs has been studied extensively by analytical [3]–[7] and compact models [8]–[10], but a much more detailed treatment of the dominant scattering processes [11]–[14] and a consideration of multidimensional quantum transport [15]–[18] will be indispensable in exploring an ultimate device performance of Si-MOSFETs.

A schematic diagram representing how to determine a current drive in the quasi-ballistic model is shown in Fig. 1. The source is treated as a reservoir of thermal carriers, which injects carriers from source to forward channel with an injection velocity of  $v_{inj}$ . When scattering exists in the channel, an average

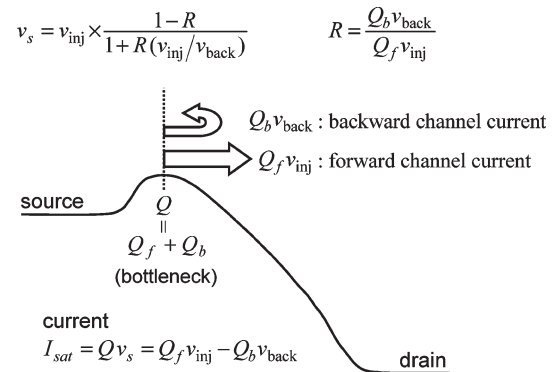


Fig. 1. Schematic diagram representing how to determine current drive in quasi-ballistic model.  $Q_f$  and  $Q_b$  are the forward and backward channel charge densities, respectively, and  $Q = Q_f + Q_b$  represents the total charge density at the bottleneck point, which is related to a sheet carrier density  $N_s^{source}$  by  $Q = eN_s^{source}$ .

carrier velocity at the source-channel barrier  $v_s$  decreases from  $v_{inj}$  and is expressed as [4]

$$v_s = v_{inj} \times \frac{1 - R}{1 + R(v_{inj}/v_{back})} \quad (1)$$

where  $v_{back}$  is a backward channel velocity and  $R$  a backscattering coefficient defined as a flux ratio given by  $R = Q_b v_{back}/Q_f v_{inj}$ , where  $Q_f$  and  $Q_b$  are the forward and the backward channel charge densities, respectively. Equation (1) is derived from the relations  $Q v_s = Q_f v_{inj} - Q_b v_{back}$  and  $Q = Q_f + Q_b$  (the carrier charge density around the bottleneck). In the ballistic limit ( $R = 0$ ),  $v_s = v_{inj}$ . As far as we know, a physical mechanism creating  $v_{inj}$  and roles of backscattering in (1) have not been fully understood yet. In this paper, we discuss these issues based upon a quantum-corrected Monte Carlo (MC) device simulation and propose a picture of quasi-ballistic transport in nanoscale MOSFETs.

## II. QUANTUM-CORRECTED MC METHOD

The MC method is a powerful tool in investigating carrier transport with various scattering processes in ultrasmall Si-MOSFETs. Lately, the quantum mechanical effects can be incorporated in the MC method by considering a quantum correction of potential in the equations of motion [12], [13],

Manuscript received June 13, 2006; revised September 18, 2006. This work was supported by the NEDO/MIRAI project. The review of this paper was arranged by Editor M. Reed.

The authors are with the Department of Electrical and Electronics Engineering, Kobe University, Kobe 657-8501, Japan (e-mail: tsuchiya@eedept.kobe-u.ac.jp).

Digital Object Identifier 10.1109/TED.2006.885672

[17]–[24]. In this paper, we employ a density-gradient-based quantum correction approach, which has been proposed by our group, as follows [12], [13], [17], [19]:

$$\frac{d\mathbf{r}}{dt} = \mathbf{v} \quad (2)$$

$$\frac{d\mathbf{k}}{dt} = -\frac{1}{\hbar} \nabla_{\mathbf{r}} (U + U_{\nu}^{\text{QC}}). \quad (3)$$

The velocity equation (2) is the same as the one used in the standard MC technique, but the force equation (3) is modified in the quantum transport so that particles evolve under the enforcement not only by the classical built-in potential  $U$  but also by the quantum correction of potential  $U_{\nu}^{\text{QC}}$  given by [12], [13], [17]

$$U_{\nu}^{\text{QC}} = -\frac{\hbar^2}{12m_x^{\nu}} \frac{\partial^2 \ln(n_{\nu})}{\partial x^2} - \frac{\hbar^2}{12m_y^{\nu}} \frac{\partial^2 \ln(n_{\nu})}{\partial y^2} - \frac{\hbar^2}{12m_z^{\nu}} \frac{\partial^2 \ln(n_{\nu})}{\partial z^2} \quad (4)$$

where the index  $\nu = (1, 2, \dots, 6)$  denotes the six equivalent valleys of the silicon conduction band.  $n_{\nu}$  represents the carrier density, and  $m_x^{\nu}$ ,  $m_y^{\nu}$ , and  $m_z^{\nu}$  represent the effective masses of the ellipsoidal bandstructure. To prevent a divergence of  $U_{\nu}^{\text{QC}}$ , the carrier density  $n_{\nu}$  is time-averaged for several 10 ps during the particle MC simulations. In addition, we adopt a smoothing technique for the quantum potential  $U + U_{\nu}^{\text{QC}}$  by using the nearest neighbor spatial points. Further, we should pay attention if we apply (4) to a carrier transport simulation at the Si/SiO<sub>2</sub> interface. Namely, the carrier density at the interface usually becomes very small due to a large potential barrier, and thus, the second-order space derivative of the carrier density tends to diverge at the interface. To overcome this problem, we introduce a coupled method with an effective potential approach [18], [20]. In the coupled method, the quantum correction of potential  $U_{\nu}^{\text{QC}}$  is used only for the Si region, while the effective potential is employed for the SiO<sub>2</sub> region [17]. In the calculation of the transition rates of the scattering processes, the quantum correction of potential  $U_{\nu}^{\text{QC}}$  should be taken into account in the evaluation of the carrier's total energy.

As compared with the alternative quantum-corrected MC approaches [18], [20], [22]–[24], the features of the density-gradient quantum correction in the MC technique are as follows: 1) parameter-free. The effective masses in (4) are given by using the standard values of  $m_l = 0.98m_0$  and  $m_t = 0.19m_0$ ; 2) simple. The solution of the Schrödinger equation is unnecessary throughout the simulation; and 3) applicability. Since the quantized subband splitting in the ellipsoidal multivalleys of the Si conduction band is accurately simulated [12], [13], we can apply it for ultrathin silicon-on-insulator (SOI) structures with Si thicknesses thinner than 10 nm. Therefore, we expect that quantum transport in ultimately scaled Si-MOSFETs can be accurately simulated by using the density-gradient-based quantum correction once we could overcome concerns relating to the density fluctuations [17], [23]. The validity of our quantum-corrected MC method mentioned above has

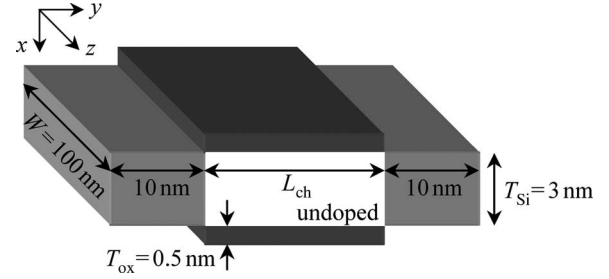


Fig. 2. Three-dimensional DG-MOSFET used in the simulation.  $T_{\text{Si}} = 3$  nm and  $T_{\text{ox}} = 0.5$  nm. The donor concentration in the source and drain regions is  $N_D = 1.0 \times 10^{20} \text{ cm}^{-3}$ , and the channel region is assumed to be undoped.

been demonstrated by comparing the one-dimensional (1-D) self-consistent Schrödinger–Poisson solution [12], [13] and the nonequilibrium Green's function approach [25].

The 3-D device model used in the simulation is shown in Fig. 2. Since the suppression of short-channel effect is crucial in a precise analysis of nanoscale MOSFETs, we adopted a double-gate (DG) and ultrathin body structure, as shown in Fig. 2. The Si body thickness  $T_{\text{Si}}$  is set as 3 nm, which is much smaller than the one used in [14], where most of the electrons propagate in the two-fold valleys with a higher mobility along the interface and phonon scattering between the subbands is forbidden [26]. Therefore, the present simulation is well suited for highly accurate investigation on the ultimate device performance of ballistic MOSFETs. Furthermore, the extremely thin gate oxide of  $T_{\text{ox}} = 0.5$  nm is adopted, which is also effective in eliminating the short-channel effect. For simplicity, the gate tunneling effect is neglected in this paper. The channel length  $L_{\text{ch}}$  is varied from 50 to 8 nm, where we confirmed that the short-channel effect is sufficiently suppressed until  $L_{\text{ch}} = 8$  nm. The device width  $W$  is given as 100 nm. The donor concentration in the source and drain regions is  $N_D = 1.0 \times 10^{20} \text{ cm}^{-3}$ , and the channel region is assumed to be undoped. The temperature is 300 K. The Poisson's equation is self-consistently solved with a 2-D carrier density averaged over the  $z$ -direction. The scattering processes considered, which play an important role in the quasi-ballistic simulation, are impurity scattering, interface roughness scattering, intravalley acoustic phonon and intervalley phonon scatterings including  $f$ - and  $g$ -phonons, and electron–electron scatterings including electron-plasmon and short-range Coulomb interactions. The impurity scattering, which is considered only in the source and drain regions, is treated by using the Brooks–Herring model for simplicity. The values of the deformation potentials and the phonon frequencies are taken from the study in [27]. The roughness scattering at the gate oxide interfaces is modeled as a mixture of specular reflections and elastic diffusions, each occurring with a probability of 0.5 at every hitting interfaces [28]. The electron–electron scatterings are incorporated by splitting the Coulomb interactions into short-range and long-range potentials, where the short-range part is included through an addition of a molecular-dynamics (MD) loop and the long-range part is treated as an additional scattering mechanism, that is, inelastic electron-plasmon scattering [13].

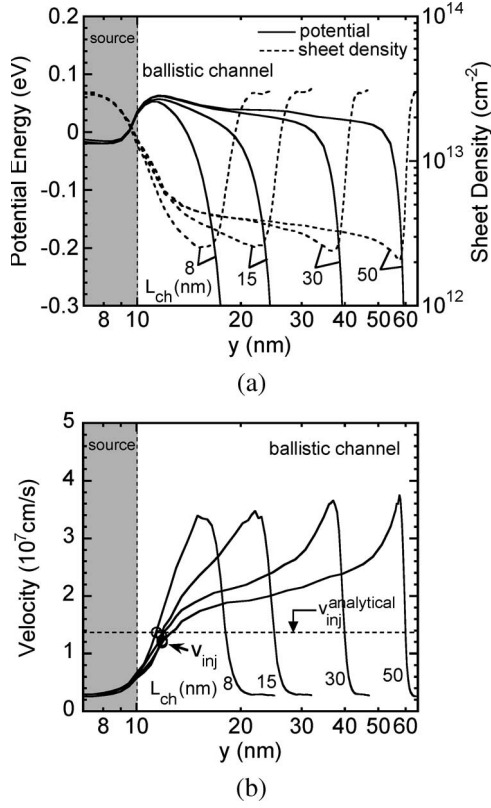


Fig. 3. (a) Potential and sheet electron concentration and (b) average electron velocity profiles along the channel computed for ballistic DG-MOSFETs with various channel lengths.  $V_{DS} = 0.6$  V (current saturation region), and  $V_G$  is adjusted to keep the sheet electron concentration  $N_s$  equal to  $7 \times 10^{12} \text{ cm}^{-2}$  at the potential bottleneck point. The scattering in the source and drain regions is considered. The horizontal dashed line represents the injection velocity calculated by using the analytical model.

The longitudinal and transverse effective masses of the silicon conduction band are explicitly considered by using the Herring–Vogt transformation. The nonparabolicity of the band-structure is taken into account by introducing a nonparabolicity parameter  $\alpha$  [27]. The degeneracy effects are also incorporated in a way that a distribution function  $f_\nu(\mathbf{k}, \mathbf{r})$  is tabulated at each location throughout the device and any scattering processes are rejected if the final electron state and band index  $\nu$  are such that  $1 - f_\nu(\mathbf{k}, \mathbf{r}) \leq \eta$ , where  $\eta$  is a random number in  $[0, 1]$ . In this paper, we apply the quantum-corrected MC and MD approaches to quasi-ballistic transport simulation in the DG-MOSFET shown in Fig. 2.

### III. SIMULATED RESULTS

#### A. Injection Velocity $v_{inj}$

To investigate a physical mechanism creating  $v_{inj}$ , we first performed a ballistic MC simulation, which means that the scattering is neglected in the channel region, while the scatterings in the source and drain regions are considered.

Fig. 3 shows the electron-transport properties computed for the fictitious ballistic MOSFETs with various channel lengths, where the source–drain voltage  $V_{DS} = 0.6$  V (current saturation region) and the gate voltage  $V_G$  is adjusted to keep the sheet

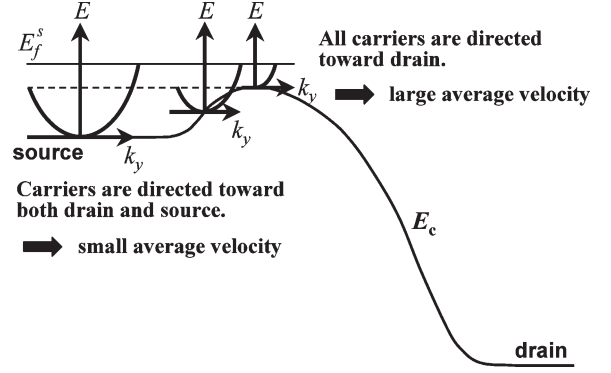


Fig. 4. Schematic diagram explaining the increase in average electron velocity at the source-end of the channel.

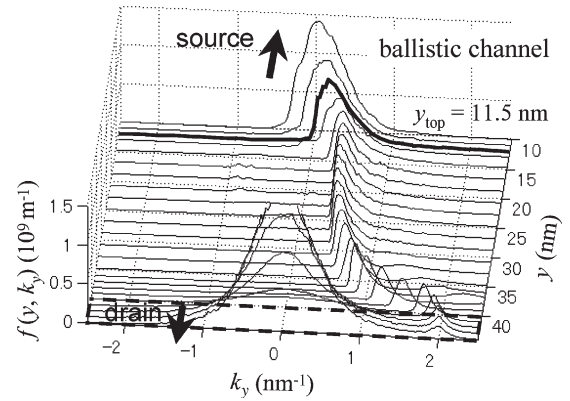


Fig. 5. Distribution function in momentum space computed for ballistic MOSFET, with  $L_{ch} = 30$  nm. The channel region extends from  $y = 10$  to  $40$  nm. The potential bottleneck is located at  $y = 11.5$  nm.

electron concentration  $N_s$  equal to  $7 \times 10^{12} \text{ cm}^{-2}$  at the potential bottleneck point. Here, it should be noted that the average electron velocity increases along the channel at the source-end barrier (potential bottleneck), and the injection velocity  $v_{inj}$  is almost independent of  $L_{ch}$ . This is due to the fact that the electrons with negative velocity vectors, which represent the electrons reflected by the potential bottleneck barrier, vanish away upon approaching the potential maximum point, as schematically shown in Fig. 4. Since the potential bottleneck barrier in the ballistic MOSFETs is almost unchanged with  $L_{ch}$ , as shown in Fig. 3(a),  $v_{inj}$  becomes independent of  $L_{ch}$ . Fig. 5 shows the computed momentum distribution function for the ballistic MOSFET with  $L_{ch} = 30$  nm, where the channel region extends from  $y = 10$  to  $40$  nm. The thick solid line indicates the distribution function at the potential bottleneck point. It is found that the distribution function having negative velocity vectors rapidly decays in a few nanometers at the source-end of the channel. As a result, an asymmetric distribution function is formed at the source-end, and thus, the average electron velocity increases as mentioned above.

To examine the shape of Fig. 5 more closely, the distribution functions at the inside of the source and at the potential bottleneck point are shown in Fig. 6(a) and (b), respectively. Here, the open circles in Fig. 6(a) and (b) indicate the symmetric and the asymmetric Fermi–Dirac functions integrated with respect

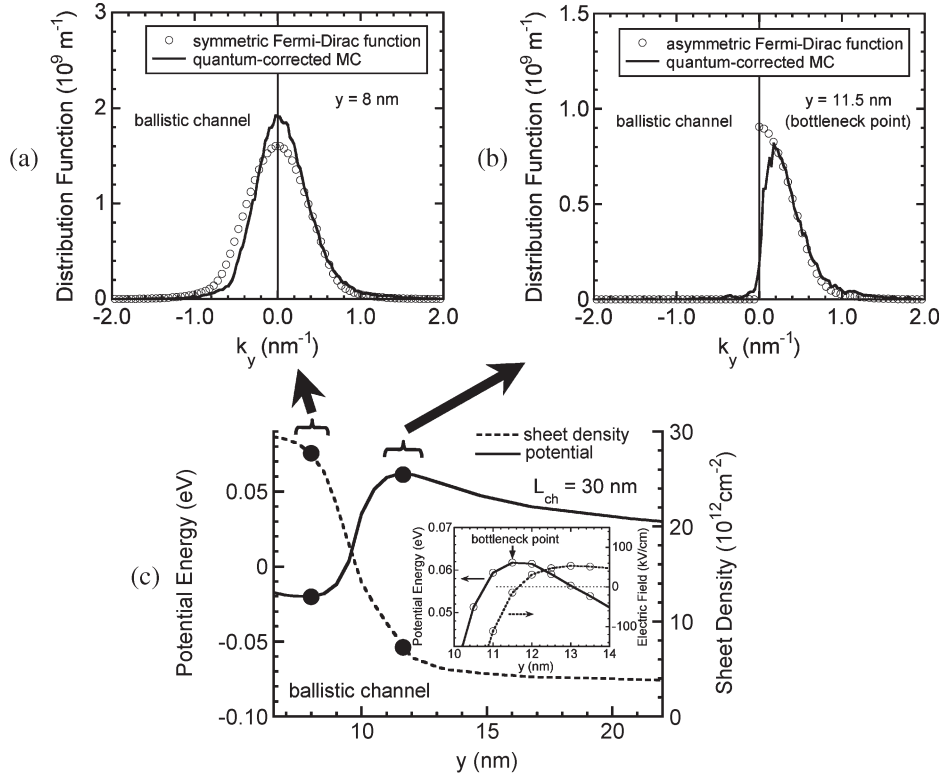


Fig. 6. Distribution functions at: (a)  $y = 8$  and (b)  $11.5 \text{ nm}$  of Fig. 5. The open circles in (a) and (b) denote the symmetric and the asymmetric Fermi-Dirac functions, respectively, and (c) represents the magnified profiles of the corresponding potential and sheet electron density, where the inset indicates the electric field distribution with spatial mesh points denoted by the open circles.

to  $k_z$ , respectively, which are calculated by using the following equation:

$$\begin{aligned}
 f_{\text{FD}}(k_y) &= \sum_{\nu=1}^6 \sum_{n_x=1}^{20} \frac{1}{\pi} \\
 &\times \int dk_z \frac{1}{1 + \exp \{ [E_x^{n_x, \nu} + E_y(k_y) + E_z(k_z) - e\phi_{\text{FS}}] / k_B T \}} \\
 &= \sum_{\nu=1}^6 \sum_{n_x=1}^{20} \frac{\sqrt{2m_z^{\nu} k_B T}}{\pi \hbar} F_{-1/2}([e\phi_{\text{FS}} - E_x^{n_x, \nu} - E_y(k_y)] / k_B T)
 \end{aligned} \quad (5)$$

where  $F_{-1/2}$  denotes the  $-1/2$ -order Fermi-Dirac integral represented by the Fermi energy  $e\phi_{\text{FS}}$ , the quantized energy levels  $E_x^{n_x, \nu}$ , and the free kinetic energy  $E_y(k_y)$ .  $e\phi_{\text{FS}}$  and  $E_x^{n_x, \nu}$  were obtained by solving the 1-D Schrödinger-Poisson equations at the corresponding sheet electron density. An analytical model for perfectly ballistic MOSFETs discussed below usually assumes an asymmetric Fermi-Dirac function at the bottleneck point [3], [4]. It is found from Fig. 6(a) that the distribution function is quasi-symmetric inside the source because of the thermalization by the scattering. On the other hand, the asymmetric distribution function without negative momentum is formed at the bottleneck point, as shown in Fig. 6(b). The asymmetric distribution function obtained from the MC simulation agrees well with the hemi-Fermi-Dirac function denoted by the open circles. The discrepancy from a discontinuous shape at zero momentum is considered to be due

to a nonnegligible driving force at the potential maximum point shown in the inset of Fig. 6(c), which is unavoidable in the finite difference scheme used in our MC simulation.

We also compared with an injection velocity estimated from the analytical model for perfectly ballistic MOSFETs proposed by Natori [3], [4]. The horizontal dashed line in Fig. 3(b) represents the injection velocity calculated by using the analytical model based upon the asymmetric Fermi-Dirac function, where we considered the twenty quantized energy levels from the lowest one for both the two-fold and four-fold valleys. It is found for the first time that the injection velocity from the analytical model  $v_{\text{inj}}^{\text{analytical}}$  corresponds well to the injection velocities obtained by using the quantum-corrected MC simulation. The above result means that the analytical model based upon the asymmetric Fermi-Dirac function is valid for the estimation of injection velocity and saturation current in perfectly ballistic MOSFETs. Incidentally, if the quantum corrections are not included, the estimated injection velocity will be underestimated for the identical electron density because the dominant electron transport in the two-fold valleys with the higher mobility along the interface is not taken into account.

### B. Roles of Backscattering

Next, we discuss the influences of scattering. Fig. 7 shows the electron-transport properties computed for the real MOSFETs with various channel lengths, where the “real” means that the scattering in the channel is considered. The bias conditions are the same as in the previous section. First, it is found that the average electron velocity at the bottleneck point  $v_s$  depends on the



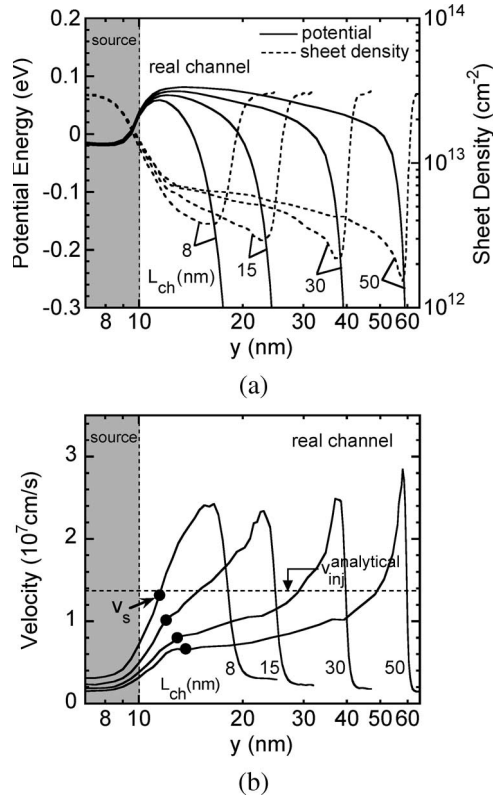


Fig. 7. (a) Potential and sheet electron concentration and (b) average electron velocity profiles along the channel computed for real DG-MOSFETs with various channel lengths, where the “real” means that scattering in the channel is considered. The bias conditions are the same as in Fig. 3. The horizontal dashed line represents the injection velocity calculated by using the analytical model.

channel length for the real MOSFETs. In other words, as shown in Fig. 8,  $v_s$  increases as  $L_{ch}$  reduces, where the solid and the open circles represent the results for the real and the ballistic MOSFETs, respectively. The numbers denote the averaged frequencies of scattering events that electrons encounter during their flight through the channel region (percentage of ballistic electrons). It is clearly found that, when the channel length becomes shorter than 30 nm, the average electron velocity at the source-end of the channel enhances according to the increase in ballistic electrons, and then it approaches the ballistic limit in the sub-10-nm regime.

Next, Fig. 9 shows the computed momentum distribution functions for the real MOSFETs with: (a)  $L_{ch} = 30$  nm and (b) 8 nm, where the channel region extends from  $y = 10$  to 40 nm in (a) and from  $y = 10$  to 18 nm in (b). It is found that the distribution function broadens due to the scattering in the channel. However, in the case of  $L_{ch} = 8$  nm, the rapid decay in the negative velocity vectors is observed at the source-end in Fig. 9(b). Consequently, the average electron velocity at the source-end of the channel approaches the ballistic limit ( $v_{inj}$ ) in the sub-10-nm regime, where stationary effects such as high-field velocity saturation will be less relevant to the device operation.

Furthermore, the roles of backscattering in the form of distribution function are shown in Fig. 10 at the potential bottleneck point, where the channel length is: (a) 30 and (b) 8 nm. The solid and the dashed lines correspond to the results for the

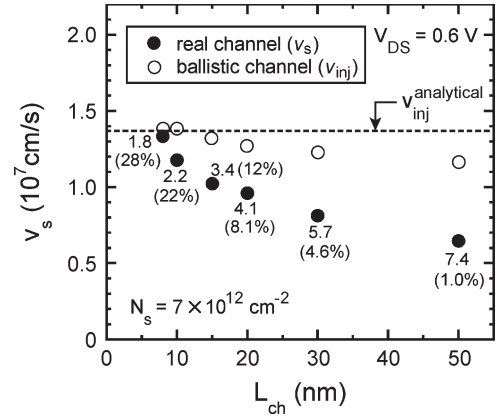


Fig. 8. Channel-length dependences of average electron velocity at the potential bottleneck point, where the solid and open circles represent the results for the real and ballistic MOSFETs, respectively. The numbers denote the averaged frequencies of scattering events in the channel region (percentage of ballistic electrons). Note that scattering events due to the short-range Coulomb interactions using MD routine are not included in these statistics.

real and the ballistic MOSFETs, respectively. Here, it should be emphasized that the increase in the negative momentum denotes the presence of backward channel current due to the scattering, while the decrease in the positive momentum is to keep the electron concentration induced by the gate bias, which represent the qualitative roles of the numerator and the denominator in (1), respectively. This may be simply called the thermalization effects by scattering at the source-end of the channel. As a result, the distribution function broadens, and the average electron velocity decreases. We notice that the thermalization by scattering becomes less significant for  $L_{ch} = 8$  nm.

Finally, we evaluated the index of ballistics  $r_B$  and backscattering coefficient  $R$  as a function of  $L_{ch}$ , as shown in Fig. 11, where  $r_B = v_s/v_{inj}$  and  $R$  is calculated by using the following equation, which was derived from (1), and the results of Fig. 8:

$$R = \frac{v_{inj} - v_s}{v_{inj} + v_s(v_{inj}/v_{back})}. \quad (6)$$

In this paper, we actually calculated the average backward channel velocity  $v_{back}$  by using the distribution function obtained from the MC simulation and found that  $v_{back} \approx 0.6 \sim 0.8v_{inj}$  for the channel lengths used in the present paper, which corresponds well to the value of  $v_{back} \approx 0.7v_{inj}$  reported in [14]. It is found from Fig. 11 that  $r_B$  approaches 1.0 and  $R$  reduces down to less than 5% in the sub-10-nm regime. In Fig. 11, the backscattering coefficients estimated by using an assumption of  $v_{back} = v_{inj}$  [5] are also plotted in the dashed line. We found that the backscattering coefficients are overestimated by about 15% with this assumption. We also notice that both  $r_B$  and  $R$  curves indicate a plateaulike behavior around  $L_{ch} = 15$  nm, which is considered to be due to a scattering rate increase for the quasi-ballistic electrons with higher kinetic energies. The above results mean that the fraction of electrons backscattered into the source electrode, which actually degrades the drive current, become less than 5% in the sub-10-nm MOSFETs, although more than 70% electrons are scattered at least once during their flight through the channel, as shown in Fig. 8.

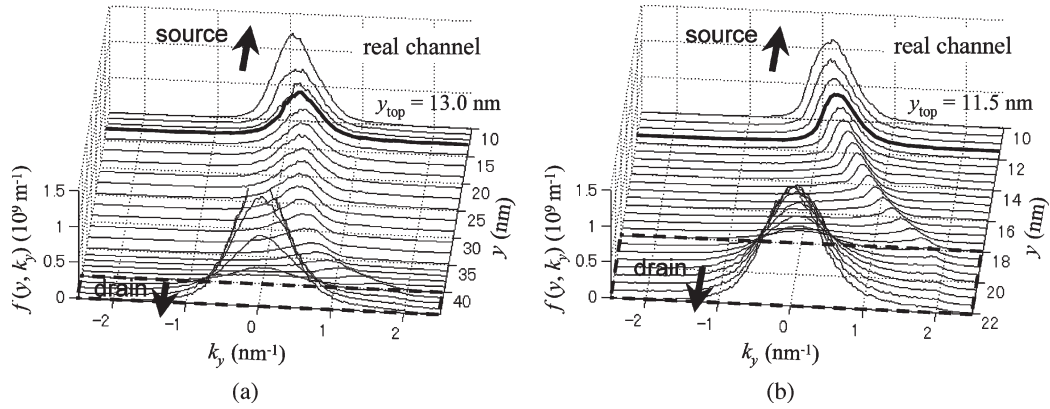


Fig. 9. Distribution functions in the momentum space computed for the real MOSFETs with: (a)  $L_{ch} = 30$  and (b) 8 nm, where the channel region extends from  $y = 10$  to 40 nm in (a) and from  $y = 10$  to 18 nm in (b).

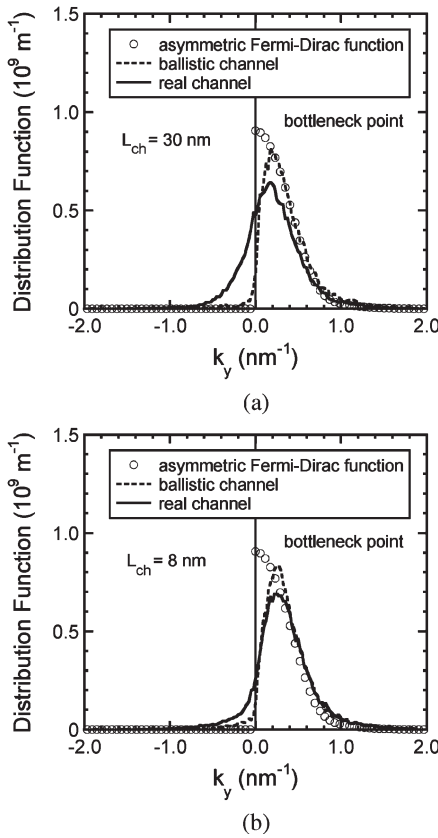


Fig. 10. Roles of backscattering in the form of distribution function at the potential bottleneck point, where the channel length is: (a) 30 and (b) 8 nm. The solid and dashed lines correspond to the results for the real and ballistic MOSFETs, respectively, and the open circles denote the asymmetric Fermi-Dirac function.

#### IV. CONCLUSION

Based upon the quantum-corrected MC device simulation, we investigated a picture of quasi-ballistic transport in nanoscale MOSFETs. First, we presented that the injection velocity at perfectly ballistic transport is independent of the channel length and corresponds well to the estimation from Natori's analytical model. Next, we demonstrated how the asymmetric momentum distribution function is formed at the bottleneck point, which was due to the fact that the carriers reflected by the potential bottleneck barrier vanish away upon

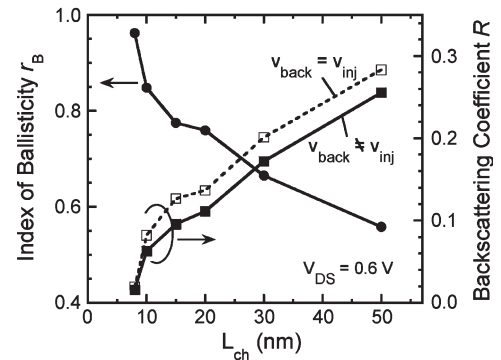


Fig. 11. Index of ballistics  $r_B$  and backscattering coefficient  $R$  calculated as a function of  $L_{ch}$ , where  $r_B = v_s/v_{inj}$ . We found that  $v_{back} \approx 0.6 \sim 0.8v_{inj}$ .

approaching the potential maximum point. We also demonstrated that the assumption of  $v_{back} = v_{inj}$  is not correct in a precise sense and overestimates the backscattering coefficient. Finally, we found that the electron velocity enhancement due to the quasi-ballistic transport will be expected as the channel length becomes shorter than 30 nm, but it will reach the ballistic limit in the sub-10-nm regime.

We will further study on backscattering localization and its effects on a drain current degradation based upon the quantum-corrected MC technique.

#### ACKNOWLEDGMENT

The authors would like to thank Prof. S. Takagi of the University of Tokyo for his valuable discussions.

#### REFERENCES

- [1] [Online]. Available: <http://www.itrs.net/Links/2005ITRS/Home2005.htm>
- [2] H. Wakabayashi, S. Yamagami, N. Ikezawa, A. Ogura, M. Narihiro, K. Arai, Y. Ochiai, K. Takeuchi, T. Yamamoto, and T. Mogami, "Sub-10-nm planar-bulk-CMOS devices using lateral junction control," in *IEDM Tech. Dig.*, 2003, pp. 989–991.
- [3] K. Natori, "Ballistic metal-oxide-semiconductor field effect transistor," *J. Appl. Phys.*, vol. 76, no. 8, pp. 4879–4890, Oct. 1994.
- [4] —, "Scaling limit of the MOS transistor—A ballistic MOSFET—," *IEICE Trans. Electron.*, vol. E84-C, no. 8, pp. 1029–1036, 2001.
- [5] M. Lundstrom, "Elementary scattering theory of the Si MOSFET," *IEEE Electron Device Lett.*, vol. 18, no. 7, pp. 361–363, Jul. 1997.

- [6] J.-H. Rhew, Z. Ren, and M. Lundstrom, "A numerical study of ballistic transport in a nanoscale MOSFET," *Solid State Electron.*, vol. 46, no. 11, pp. 1899–1906, Nov. 2002.
- [7] A. Rahman, J. Guo, S. Datta, and M. Lundstrom, "Theory of ballistic nanotransistors," *IEEE Trans. Electron Devices*, vol. 50, no. 9, pp. 1853–1864, Sep. 2003.
- [8] E. Fuchs, P. Dullfus, G. L. Carval, S. Barraud, D. Villanueva, F. Salvetti, H. Jaouen, and T. Skotnicki, "A new backscattering model giving a description of the quasi-ballistic transport in nano-MOSFET," *IEEE Trans. Electron Devices*, vol. 52, no. 10, pp. 2280–2289, Oct. 2005.
- [9] G. Curatola, G. Doornbos, J. Loo, Y. V. Ponomarev, and G. Iannaccone, "Detailed modeling of sub-100-nm MOSFETs based on Schrödinger DD per subband and experiments and evaluation of the performance gap to ballistic transport," *IEEE Trans. Electron Devices*, vol. 52, no. 8, pp. 1851–1858, Aug. 2005.
- [10] G. Mugnaini and G. Iannaccone, "Physics-based compact model of nanoscale MOSFETs—Part I: Transition from drift-diffusion to ballistic transport," *IEEE Trans. Electron Devices*, vol. 52, no. 8, pp. 1795–1801, Aug. 2005.
- [11] A. Svizhenko and M. Anantram, "Role of scattering in nanotransistors," *IEEE Trans. Electron Devices*, vol. 50, no. 6, pp. 1459–1466, Jun. 2003.
- [12] H. Tsuchiya, M. Horino, M. Ogawa, and T. Miyoshi, "Quantum transport simulation of ultrathin and ultrashort silicon-on-insulator metal-oxide-semiconductor field-effect transistors," *Jpn. J. Appl. Phys.*, vol. 42, no. 12, pp. 7238–7243, Dec. 2003.
- [13] H. Tsuchiya, A. Oda, M. Ogawa, and T. Miyoshi, "A quantum-corrected Monte Carlo and molecular dynamics simulation on electron-density-dependent velocity saturation in silicon metal-oxide-semiconductor field-effect transistors," *Jpn. J. Appl. Phys.*, vol. 44, no. 11, pp. 7820–7826, 2005.
- [14] P. Palestri, D. Esseni, S. Eminent, C. Fiegna, E. Sangiorgi, and L. Selmi, "Understanding quasi-ballistic transport in nano-MOSFETs: Part I—Scattering in the channel and in the drain," *IEEE Trans. Electron Devices*, vol. 52, no. 12, pp. 2727–2735, Dec. 2005.
- [15] A. Svizhenko, M. Anantram, T. Govindan, and B. Biegel, "Two-dimensional quantum mechanical modeling of nanotransistors," *J. Appl. Phys.*, vol. 91, no. 4, pp. 2343–2354, Feb. 2002.
- [16] Z. Ren, R. Venugopal, S. Goasguen, S. Datta, and M. Lundstrom, "nanoMOS2.5: A two-dimensional simulator for quantum transport in double-gate MOSFETs," *IEEE Trans. Electron Devices*, vol. 50, no. 9, pp. 1914–1925, Sep. 2003.
- [17] M. Ogawa, H. Tsuchiya, and T. Miyoshi, "Quantum electron transport modeling in nano-scale devices," *IEICE Trans. Electron.*, vol. E86-C, no. 3, pp. 363–371, 2003.
- [18] D. Ferry, R. Akis, and D. Vasileska, "Quantum effects in MOSFETs: Use of an effective potential in 3D Monte Carlo simulation of ultra-short channel devices," in *IEDM Tech. Dig.*, 2000, pp. 287–290.
- [19] H. Tsuchiya and T. Miyoshi, "Quantum transport modeling of ultra-small semiconductor devices," *IEICE Trans. Electron.*, vol. E82-C, no. 6, pp. 880–888, Jun. 1999.
- [20] D. Ferry, "Effective potentials and the onset of quantization in ultrasmall MOSFETs," *Superlattices Microstruct.*, vol. 28, no. 5/6, pp. 419–423, Nov. 2000.
- [21] H. Tsuchiya and U. Ravaioli, "Particle Monte Carlo simulation of quantum phenomena in semiconductor nanostructures," *J. Appl. Phys.*, vol. 89, no. 7, pp. 4023–4029, Apr. 2001.
- [22] B. Winstead and U. Ravaioli, "A quantum correction based on Schrödinger equation applied to Monte Carlo device simulation," *IEEE Trans. Electron Devices*, vol. 50, no. 2, pp. 440–446, Feb. 2003.
- [23] B. Wu, T. Tang, J. Nam, and J.-H. Tsai, "Monte Carlo simulation of symmetric and asymmetric double-gate MOSFETs using Bohm-based quantum correction," *IEEE Trans. Nanotechnol.*, vol. 2, no. 4, pp. 291–294, Dec. 2003.
- [24] X.-F. Fan, X. Wang, B. Winstead, L. F. Register, U. Ravaioli, and S. K. Banerjee, "MC simulation of strained-Si MOSFET with full-band structure and quantum correction," *IEEE Trans. Electron Devices*, vol. 51, no. 6, pp. 962–970, Jun. 2004.
- [25] H. Tsuchiya, A. Svizhenko, M. Anantram, M. Ogawa, and T. Miyoshi, "Comparison of non-equilibrium Green's function and quantum-corrected Monte Carlo approaches in nano MOS simulation," *J. Comput. Electron.*, vol. 4, no. 1/2, pp. 35–38, 2005.
- [26] S. Takagi, J. Koga, and A. Toriumi, "Mobility enhancement of SOI MOSFETs due to subband modulation in ultrathin SOI films," *Jpn. J. Appl. Phys.*, vol. 37, no. 3B, pp. 1289–1294, Mar. 1998.
- [27] C. Jacoboni and L. Reggiani, "The Monte Carlo method for the solution of charge transport in semiconductors with applications to covalent materials," *Rev. Mod. Phys.*, vol. 55, no. 3, pp. 645–705, Jul. 1983.

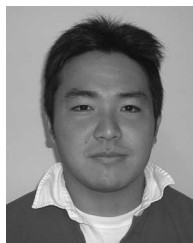
- [28] M. V. Fischetti and S. E. Laux, "Monte Carlo analysis of electron transport in small semiconductor devices including band-structure and space-charge effects," *Phys. Rev. B, Condens. Matter*, vol. 38, no. 14, pp. 9721–9745, Nov. 1988.



**Hideaki Tsuchiya** (M'93–SM'01) was born in Ehime, Japan, on August 12, 1964. He received the B.S., M.S., and Ph.D. degrees all in electronic engineering from Kobe University, Kobe, Japan, in 1987, 1989, and 1993, respectively.

In 1993, he joined the Department of Electrical and Electronics Engineering, Kobe University, as a Research Associate. He has been engaged in the research of quantum transport simulation of mesoscopic devices. From 1999 to 2000, he was a Visiting Scientist with the University of Illinois at Urbana-Champaign. In 2003, he became an Associate Professor with Kobe University. His current research includes the quantum transport modeling in nanoscale MOSFETs and the first-principles simulation in atomic-scale devices.

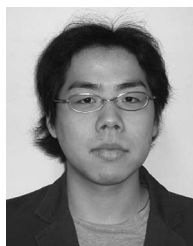
Dr. Tsuchiya is a member of the Institute of Electronics, Information and Communication Engineers of Japan, and the Japan Society of Applied Physics. He received a Young Scientist Award in 1998 from the Japan Society of Applied Physics and an Outstanding Achievement Award for a pioneering research on nanoscale device simulator in 2006 from the Institute of Electronics, Information and Communication Engineers of Japan.



**Kazuya Fujii** was born in Kyoto, Japan, on August 16, 1982. He received the B.S. degree in electrical and electronics engineering from Kobe University, Kobe, Japan, in 2005, where he is currently working toward the M.S. degree.

His research involves three-dimensional Monte Carlo device simulation with quantum corrections in nanoscale and nanowire MOSFETs.

Mr. Fujii is a member of the Japan Society of Applied Physics.



**Takashi Mori** was born in Kobe, Japan, on April 2, 1982. He received the B.S. degree in electrical and electronics engineering from Kobe University, in 2006, where he is currently working toward the M.S. degree.

His research involves Monte Carlo device simulation with quantum corrections in MOSFETs, including new channel materials.



**Tanroku Miyoshi** (S'67–M'72) was born in Osaka, Japan, on January 6, 1944. He received the B.S., M.S., and Ph.D. degrees all in electronic engineering from University of Tokyo, Tokyo, Japan, in 1967, 1969, and 1972, respectively.

In 1972, he was appointed Lecturer, and from 1974 to 1987, he was an Associate Professor with the Department of Electronic Engineering, Kobe University, Kobe, Japan, where he is presently a Professor. He has been engaged in the research of electromagnetic wave theory, microwave integrated circuits, and lightwave electronics. In 1976, he was a Visiting Scholar with the McGill University, Montreal, PQ, Canada. From 1982 to 1984, he was a Visiting Scientist with Bell Laboratories, Holmdel, NJ. His current research includes the quantum transport modeling in nanoscale devices.

Dr. Miyoshi is a member of the Institute of Electronics, Information and Communication Engineers of Japan and the Japan Society of Applied Physics. He received a Yonezawa Award in 1974, an Outstanding Book Award in 1977, and an Outstanding Achievement Award for a pioneering research on nanoscale device simulator in 2006 all from the Institute of Electronics, Information and Communication Engineers of Japan.